



Investigating the impact of advective and diffusive controls in solute transport on geoelectrical data

Daniel D. Wheaton, Kamini Singha*

Department of Geosciences, Pennsylvania State University, University Park, Pennsylvania, 16802, USA

ARTICLE INFO

Article history:

Received 1 July 2009

Accepted 13 June 2010

Keywords:

Solute transport
Dual-domain mass transfer
Electrical resistivity
COMSOL

ABSTRACT

Multiple types of physical heterogeneity have been suggested to explain anomalous solute transport behavior, yet determining exactly what controls transport at a given site is difficult from concentration histories alone. Differences in timing between co-located fluid and bulk apparent electrical conductivity data have previously been used to estimate solute mass transfer rates between mobile and less-mobile domains; here, we consider if this behavior can arise from other types of heterogeneity. Numerical models are used to investigate the electrical signatures associated with large-scale hydraulic conductivity heterogeneity and small-scale dual-domain mass transfer, and address issues regarding the scale of the geophysical measurement. We examine the transport behavior of solutes with and without dual-domain mass transfer, in: 1) a homogeneous medium, 2) a discretely fractured medium, and 3) a hydraulic conductivity field generated with sequential Gaussian simulation. We use the finite-element code COMSOL Multiphysics to construct two-dimensional cross-sectional models and solve the coupled flow, transport, and electrical conduction equations. Our results show that both large-scale heterogeneity and subscale heterogeneity described by dual-domain mass transfer produce a measurable hysteresis between fluid and bulk apparent electrical conductivity, indicating a lag between electrical conductivity changes in the mobile and less-mobile domains of an aquifer, or mass transfer processes, at some scale. The shape and magnitude of the observed hysteresis is controlled by the spatial distribution of hydraulic heterogeneity, mass transfer rate between domains, and the ratio of mobile to immobile porosity. Because the rate of mass transfer is related to the inverse square of a diffusion length scale, our results suggest that the shape of the hysteresis curve is indicative of the length scale over which mass transfer is occurring. We also demonstrate that the difference in sampling scale between fluid conductivity and geophysical measurements is not responsible for the observed hysteresis. We suggest that there is a continuum of hysteresis behavior between fluid and bulk electrical conductivity caused by mass transfer over a range of scales from small-scale heterogeneity to macroscopic heterogeneity.

© 2010 Elsevier B.V. All rights reserved.

1. Introduction

Subsurface solute transport is classically described with the advection–dispersion equation, which assumes that transport is Fickian in nature, such that concentration observed over time at a point in space (known as a concentration history or breakthrough curve) has a nearly Gaussian distribution for a conservative solute (Bear, 1972; Berkowitz and Scher, 2001). Breakthrough curves from laboratory and field experiments over the past several decades, however, often exhibit anomalous behavior, including skewed curves, elongated tails, and/or multiple peaks (e.g., Adams and Gelhar, 1992; Levy and Berkowitz, 2003; Cortis and Berkowitz, 2004). Numerous hypotheses exist for describing this behavior, including diffusion-like

processes such as dual-domain mass transfer (e.g., Haggerty and Gorelick, 1994; Haggerty and Gorelick, 1995), time delays between the concentration gradient and mass flux from inertial effects and subscale heterogeneity (e.g., Dentz and Tartakovsky, 2006), and variable transport rates caused by large-scale heterogeneity (e.g., Becker and Shapiro, 2000; Becker and Shapiro, 2003). Several mathematical formulations such as continuous-time random-walk theory (e.g., Berkowitz and Scher, 1995) and fractional advection–dispersion equations (e.g., Benson et al., 2000) have been proposed to simulate these observed transport behaviors.

Diffusion-based processes in dual domains have been thought to control transport in some settings. For example, an advection–dispersion model could not explain all the salient features of the bromide plume, most notably the mass balance, during a tracer test in the fluvial materials at the MAcroDispersion Experiment (MADE) Site in Columbus, Mississippi. At early time, the plume mass was overestimated by 52% while at late times it was underestimated by 23% (Adams and Gelhar, 1992). Numerical simulations utilizing dual-domain mass transfer (Fig. 1), where solute diffuses between a mobile zone (the continuous path, such

* Corresponding author. 311 Deike Building, University Park, PA 16802. Tel.: +1 814 863 6649; fax: +1 814 863 7823.

E-mail addresses: danieldwheaton@gmail.com (D.D. Wheaton), ksingha@psu.edu (K. Singha).

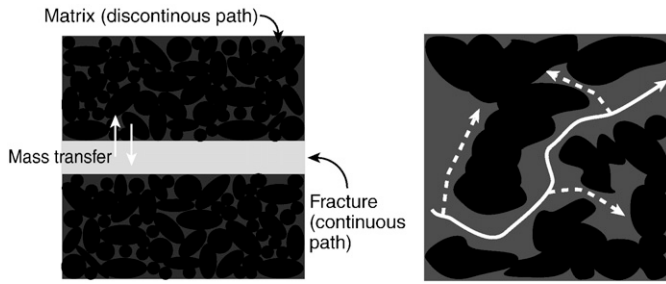


Fig. 1. Conceptual model of dual-domain mass transfer. Solute moves through two domains: the mobile zone or continuous pathway and the immobile zone or discontinuous pathway. The mass transfer rate controls the diffusive exchange of solute between the two domains. In the example on the left, the fracture represents the mobile zone while the matrix represents the immobile zone. In the example on the right, solute following the path of the solid white line would move through the mobile zone. Solute following the dotted white path would move into dead-end pore space or immobile zone and may have to diffuse back into the mobile zone.

as fractures or connected pore space) and an immobile or less-mobile zone (a discontinuous path, such as the rock matrix surrounding fractured media, or unconnected pore space), was able to accurately predict both solute migration and mass balance characteristics at the MADE site (Feehley et al., 2000; Harvey and Gorelick, 2000). Transport models controlled by advection–dispersion only were unable to explain the same behavior (Barlebo et al., 2004).

Other studies have explained an anomalous solute tailing behavior using advectively controlled transport. For example, tracer tests were conducted in a fractured-rock environment at Mirror Lake, New Hampshire, using three separate conservative tracers with different diffusion coefficients, each with two different pumping configurations (Becker and Shapiro, 2000; Becker and Shapiro, 2003). Because tracers with different diffusion coefficients produced identical late-time breakthrough behavior, the authors concluded that long tailing resulted from an advective mechanism, not a diffusive one, and proposed that the solute advects via different paths at different speeds to reach a given destination. The early arrivals represent solute that has taken the fastest route whereas the later arrivals have taken a longer way or slower path; the authors termed this behavior “heterogeneous advection”. Day-Lewis et al. (2006) supported these results by collecting a suite of saline tracer, hydraulic and time-lapse radar data at Mirror Lake, and demonstrated that heterogeneity in the permeability structure could explain their field observations. In highly heterogeneous material such as fractured-rock, anomalous transport controlled by advection is an attractive explanation.

Distinguishing between the processes controlling transport, such as heterogeneous advection based on macroscopic heterogeneity versus diffusive processes like dual-domain mass transfer, is generally based on solute concentration histories measured within the mobile domain. Unfortunately, concentration histories often do not contain enough information to distinguish between the proposed processes. Sánchez-Vila and Carrera (2004) demonstrated that for large travel distances the breakthrough-curve shape could not be used to discern between advectively controlled and diffusion-controlled transport because it is possible to choose physical parameters for both conceptual models that resulted in each one fitting the same set of temporal moments. There is consequently still some question as to when a simple advection–dispersion model should be used to reproduce the plume characteristics (Barlebo et al., 2004; Hill et al., 2006; Molz et al., 2006) and over what length scale mass transfer occurs. To accurately predict solute migration through natural systems, we must integrate new data types that may help to discriminate which processes control solute transport, and determine which models are most appropriate at a particular field site.

Geophysical methods may provide additional pertinent data in these investigations. Results from an electrical geophysical dataset obtained during an aquifer-storage and recovery (ASR) test in Charleston, South

Carolina indicate that direct-current resistivity methods may be able to help estimate mass transfer behavior in situ (Singha et al., 2007). The authors observed hysteresis between fluid electrical conductivity (EC) and the bulk apparent EC, which contradicts common rock physics relations, and suggested that the hysteresis is an effect of dual-domain mass transfer. They contended that the lag between fluid EC and bulk apparent EC is controlled by the rate of transfer between mobile and immobile zones. This observation indicates that electrical geophysical data, in conjunction with saline tracer tests, may provide evidence about scales of mass transfer in controlling solute breakthrough behavior. This conclusion was further supported by theoretical work in Day-Lewis and Singha (2008) and Singha et al. (2008).

To discriminate the processes controlling transport with geophysical methods, we need to quantify the “footprint” or support volume of the geophysical measurement. If the fluid and bulk EC data are out of equilibrium solely due to differences in support volume, then plume shape could play an important role in the interpretation of the hysteresis between bulk and fluid EC, as previous studies have shown that large, diffuse plumes can be more easily captured with electrical data than small, highly concentrated ones (Singha and Gorelick, 2006). If averaging by the geophysical method is not responsible for the disequilibrium between bulk apparent and fluid EC data, then the observed disequilibrium suggests the effect of either dual-domain mass transfer or heterogeneous advection. Geophysical data can then be used to monitor disequilibrium between subsurface domains at some effective scale. No studies have looked at this effect in detail.

Here, we use numerical models to investigate the electrical signatures of solutes associated with large-scale permeability heterogeneity and dual-domain mass transfer to determine if the behavior in geophysical data is dependent on the scale of heterogeneity or process controlling solute transport. These numerical models highlight how differences in scale and support between hydrologic and geophysical methods affect data interpretation. Below, we analyze a series of numerical experiments to understand the impacts macroscopic hydraulic conductivity heterogeneity and dual-domain mass transfer have on breakthrough curves and electrical signatures.

2. Model construction

To test how macroscopic permeability heterogeneity and dual-domain mass transfer control solute tailing behavior for simplified situations and how these processes are detected with electrical data, a coupled flow, transport and electrical conduction numerical model was constructed using COMSOL (2006). Two-dimensional, transient cross-sectional models were created to investigate solute transport from an injection well in the presence and absence of dual-domain mass transfer under a variety of geologic conditions, including: 1) homogeneous hydraulic conductivity in the subsurface, 2) discretely fractured media, and 3) highly heterogeneous hydraulic conductivity without discrete fractures in the subsurface. Hydraulic head, solute concentration, and bulk apparent EC data were simulated for each conceptual model.

We first solve a transient flow system described by:

$$S \frac{\partial H}{\partial t} + \nabla \cdot \left[-\frac{K}{(\rho_f g)} \nabla (p + \rho_f g D) \right] = Q_s \quad (1)$$

$$H = \frac{p}{(\rho_f g)} + D \quad (2)$$

where S is the storage term ($1/L$), H is hydraulic head (L), t is time (T), K is the hydraulic conductivity (L/T), ρ_f is the fluid density (M/L^3), g is the constant of gravitational acceleration (L/T^2), p is the pressure (M/LT^2), D is elevation (L), and Q_s is the source of fluid ($1/T$). For a

single domain, the predicted flow velocities from this numerical model are used to solve for concentration by:

$$\Phi_m \frac{\partial c_m}{\partial t} + \nabla \cdot (-\Phi_m D_L \nabla c_m) = -u \nabla c_m + R_L \quad (3)$$

where Φ_m is the connected porosity (dimensionless), c_m is the solute concentration in the connected pore space (M/L^3), t is time (T), D_L is the coefficient of hydrodynamic dispersion (L^2/T), u is the fluid velocity vector (L/T), and R_L is the chemical reaction of the solute in the liquid phase (M/L^3T). The form of the coefficient of hydrodynamic dispersion is:

$$D_{ii} = \alpha_L \frac{u_i^2}{\bar{u}} + \alpha_T \frac{u_j^2}{\bar{u}} + \tau_L D_{mL} \quad (4a)$$

$$D_{ji} = D_{ij} = (\alpha_L - \alpha_T) \frac{u_i u_j}{\bar{u}} \quad (4b)$$

where α_L is the dispersivity in the longitudinal flow direction (L), α_T is the dispersivity in the transverse flow direction (L), u_i are the fluid velocity components in the respective directions, τ_L is the tortuosity factor (dimensionless), and D_{mL} is the coefficient of molecular diffusion of the solute (L^2/T).

For models incorporating dual-domain mass transfer, a second equation describes that process:

$$\Phi_{im} \frac{\partial c_{im}}{\partial t} + \nabla \cdot (-\Phi_{im} D_L \nabla c_{im}) = R_L \quad (5)$$

where Φ_{im} is the immobile porosity (dimensionless) and c_{im} is the solute concentration in the immobile domain (M/L^3). In this case, the hydrodynamic dispersion term only includes molecular diffusion. The reaction term links the mobile and immobile domains, where

$$\text{for the mobile domain: } R_L = \beta(c_m - c_{im}), \text{ and} \quad (6a)$$

$$\text{for the immobile domain: } R_L = -\beta(c_m - c_{im}) \quad (6b)$$

where β is the rate of diffusive mass transfer between domains ($1/T$). We note that for the models here, only a single rate of mass transfer is used, although previous studies have used multi-rate models to account for mass transfer rates that vary with scale (e.g., Haggerty and Gorelick, 1995).

To convert estimated concentrations to electrical conductivity, we follow the relation established in Keller and Frischknecht (1966) where 1 mg/L equals 0.002 mS/cm. For models without dual-domain mass transfer, the fluid EC can be used in Archie's Law (Archie, 1942) to calculate the bulk EC:

$$\sigma_b = a \sigma_f \Phi_m^\eta \quad (7)$$

where a is a fitting parameter (dimensionless), σ_f is the fluid conductivity (mS/cm), and η is the cementation exponent (dimensionless), which is related to the geometry of the pore space and typically ranges between 1.3 and 2. In the models with dual-domain mass transfer, we follow Singha et al. (2007) to calculate the bulk EC:

$$\sigma_b = (\Phi_m + \Phi_{im})^{\eta-1} \cdot (\Phi_m \sigma_{f,m} + \Phi_{im} \sigma_{f,im}) \quad (8)$$

where $\sigma_{f,m}$ is the fluid conductivity in the mobile domain (mS/cm) and $\sigma_{f,im}$ is the fluid conductivity in the immobile domain (mS/cm). This equation is based on volumetric averaging, which is the same as a model of bulk conductivity or resistivity that assumes conductors in parallel and similar connectivity within a given domain. Other averaging may be more appropriate for random media and should be verified with laboratory studies. Additionally, differences in formation

factors between the mobile and immobile domains are not considered, as data on these properties are difficult to measure directly. These are important concerns that would change the magnitude of the electrical conductivity between domains, although not the behavior of transport outlined here. Bulk EC was then used to solve for voltage using the following equation:

$$-\nabla \cdot d(\sigma_b \nabla V - J^e) = dQ_j \quad (9)$$

where d is the thickness in the third direction into the page for these 2-D models (L), V is the electric potential (volts), J^e is the external current density (A/L^2), and Q_j is the current source (A/L^3). The electric potential is used to calculate the bulk apparent EC:

$$\sigma_{ba} = \frac{I}{(V_M - V_N) \cdot K_F} \quad (10)$$

where V_M is the electric potential at the first potential electrode (volts), V_N is the electric potential at the second potential electrode (volts), K_F is the geometric factor (L), and I is the current (A).

The model domain is 60 m tall by 100 m wide, and includes an internal area of fine meshing near the injection well and electrode locations. In this synthetic experiment, we note that the boundaries are close to the area of interest, but were determined to have a minimal effect on the resultant heads, concentrations, and voltages. An unstructured triangular mesh was generated using the built-in finite-element mesher with a predefined coarse mesh size, and was then refined. The maximum element growth rate was 50%. The top and bottom boundaries for the flow and transport simulations are no-flux boundaries. For flow, the left boundary is a specified head of 3 m, and the right boundary is a specified head of 1 m, producing a hydraulic head gradient of 0.02. For transport, the left boundary is a specified concentration of 85 mg/L. The right-hand boundary is an advective-flux condition, which allows any solute being carried by the fluid to exit the model, preventing a buildup of solute at the boundary. The background concentration was set to 85 mg/L. When dual-domain mass transfer exists within the model, the initial concentration in the immobile domain was also set to 85 mg/L. For electrical flow, all boundaries were set to an electric potential of 0 V. Parameters used in the modeling are shown in Table 1.

To evaluate the electrical response to tracer behavior, we simulate a push-pull type test, loosely mimicking the data collection procedure described in Singha et al. (2007). The injection/extraction well was represented by a series of 32 points spaced 1 m apart vertically from 9 m to 40 m below the simulated land surface and 46.5 m to the

Table 1

Physical parameters used in the homogeneous numerical models of flow, transport, and electrical conduction.

Storage term (S)	$3e-5 \text{ m}^{-1}$
Hydraulic conductivity (K)	$1.15e-4 \text{ m/s}$
Hydraulic gradient	0.02
Injection rate	0.07 L/s
Pumping rate	0.095 L/s
Total porosity (Φ_m)	0.1
Dispersivity, primary direction (mobile, α_1)	1 m
Dispersivity, secondary direction (mobile, α_2)	0.1 m
Tortuosity factor (τ_L)	1
Coefficient of molecular diffusion (D_L)	$1e-6 \text{ m}^2/\text{s}$
Initial solute concentration	85 mg/L
Injection concentration	16,000 mg/L
Current driven	1 A/m
Cementation factor	2
Mass transfer rate (β)	$1e-3/\text{day} - 1e-1/\text{day}$
Mobile porosity (Φ_m)	0.025
Immobile porosity (Φ_{im})	0.075
Dispersivity, primary direction (immobile, α_1)	0 m
Dispersivity, secondary direction (immobile, α_2)	0 m

right of the model origin, near the midpoint of the system. At these locations, we injected 16,000 mg/L of solute at a total rate of 0.07 L/s for 12 days, then ended the injection and allowed the fluid to flow due to the head gradient imposed by the boundary conditions for 2 days, and then extracted fluid at a total rate of 0.095 L/s for 32 days. The injection and pumping rates mentioned above were distributed evenly among the points representing the active well to evenly distribute the pressure and solute over the entire well. Another series of 24 points located 7 m to the right of the injection well and spaced 1 m apart vertically from 17 m to 40 m below the simulated ground surface represent the observation well and electrodes. To drive current, a given electrode pair was simulated by giving one point at the observation well a current source of 1 A/m and giving the other one a current source of -1 A/m.

Bulk apparent EC measurements were simulated with a dipole–dipole type array considering only in-well dipoles. Skip-0 to skip-2 geometries were used, where the ‘skip’ describes how many electrodes were skipped within a dipole; for a smaller skip, the measurement averages less of the subsurface and provides better resolution (Slater et al., 2000). We consider raw, uninverted bulk apparent EC data in this study, as was done in Singha et al. (2007), where apparent EC values are calculated using the injected current, voltage change between potential electrodes, and a calculated geometric factor.

Flow and transport both required transient analysis because the injection and pumping conditions are time dependent. Because the bulk apparent EC measurement and its effects are effectively instantaneous, the electrical flow only required a steady-state analysis. The flow and transport problems were solved simultaneously (strongly coupled). In the presence of dual-domain mass transfer, the second transport equation is solved as strongly coupled with the flow and transport problem. After the flow and transport simulations were finished, the steady-state electrical equation was solved through time for all the different electrode configurations. The models simulate a total of 1100 h to capture the extent of the tailing.

3. Development of a homogeneous model

To start, we consider a numerical model given the boundary and initial conditions outlined above with a homogeneous hydraulic conductivity of $1.15e-4$ m/s. In this system, we model both classic advective–dispersive behavior and dual-domain mass transfer, and explore the geophysical signature associated with both. The homogeneous model serves as a control and provides an opportunity to observe the effects of dual-domain mass transfer in the absence of heterogeneity. This model mesh was refined until the element sides were approximately 17 cm long, and ended up containing 8491 triangular elements. The models presented here have a total porosity, in both cases, of 0.1. Modeling parameters are summarized in Table 1.

3.1. Modeling classical advective–dispersive behavior

When modeling classic advective–dispersive behavior, the tracer transport appears Fickian, as expected: skip-0 bulk apparent EC in the homogeneous model behaves in accordance with classical solute transport and Archie’s Law, and fluid EC and bulk apparent EC vary linearly (Fig. 2). The bulk apparent and fluid EC at the observation well increase over time as solute breaks through, and then decrease during the pumping period as tracer is pulled back to the injection well. Although there is no heterogeneity in this scenario, we find that similar to field bulk EC data, the model results show that as electrode spacing increases, the response associated with the plume decreases. This behavior is expected because increasing the electrode spacing increases the support volume of the measurement at the expense of measurement resolution. Consequently, we deal only with skip-0 data here. However, we note that increasing the skip does not cause a disequilibrium between the fluid and bulk EC data in these

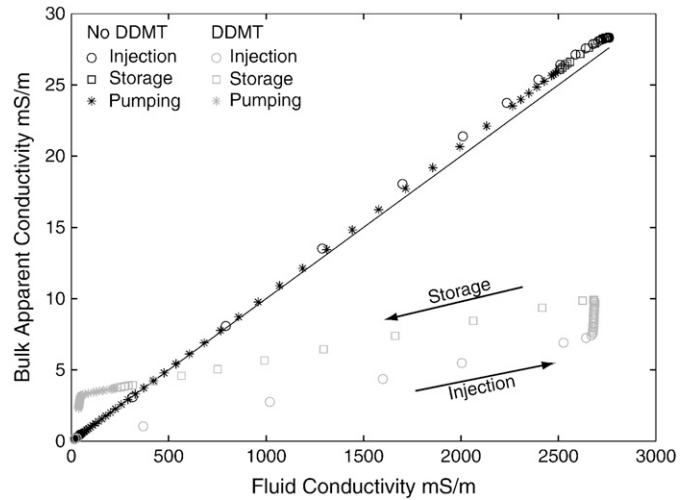


Fig. 2. Simulated bulk apparent and fluid EC for a model with homogeneous hydraulic conductivity. The black line is the true relation between bulk apparent and fluid EC used in the model. The simulated bulk apparent EC deviates from the true value as a function of support volume or geometric factor, but does not produce a measurable hysteresis when dual-domain mass transfer is not simulated (black symbols). Introducing dual-domain mass transfer (DDMT) at a rate of 10^{-3} /day (gray symbols) produces hysteresis. During the injection and storage periods, the hysteresis curve is below the true relation between fluid and bulk apparent EC because the immobile domain, which accounts for 75% of the total porosity of 0.1, is relatively fresh compared to the mobile domain. Although not shown here, the shape of the hysteresis is controlled by the rate of mass transfer and ratio of mobile to immobile porosity.

models, indicating, at least at the macroscopic scale, that the scale of measurement does not impart hysteresis without the presence of heterogeneity.

3.2. Modeling dual-domain mass transfer

Given the same parameterization as above, we add dual-domain mass transfer to our simulation. This requires the selection of two additional parameters: immobile porosity and mass transfer rate, as shown in Eqs. (5), (6a), and (6b). In these models, the immobile porosity is set to be 0.075 and the mobile porosity is set to 0.025, for the same total porosity that was used in the previous simulation. At low mass transfer rates ($<1e-3$ /day), the system behaves as a single domain and transport is approximately Fickian. By $1e-3$ /day, the results are distinct compared to a single-domain model—elongated tails exist in the breakthrough curves and significant concentration is transferred into the less-mobile domain (Fig. 3). The rate of mass transfer is equal to the diffusion divided by the length scale of mass transfer squared, so a mass transfer rate of $1e-3$ /day is equivalent to heterogeneity on the scale of ~ 9 m given a diffusion coefficient of $1e-6$ m²/s, whereas a mass transfer rather of $1e-2$ /day is equivalent to heterogeneity on the scale of ~ 3 m.

Mobile-domain concentrations in injection, storage, and early pumping periods are lower in the presence of dual-domain mass transfer than would be expected in the single-domain case due to mass being stored in the less-mobile domain (Fig. 3). During the pumping stage, mobile concentrations are higher than in the single-domain model because previously trapped solute is diffusing back into the mobile domain from an immobile domain ‘‘source’’. For rates of mass transfer greater than $1e-3$ /day, we observe a concentration rebound at the beginning of the pumping stage (Fig. 3); as the solute concentration in the mobile domain is removed, the mobile domain becomes out of equilibrium with the high solute concentration in the immobile domain. To compensate, solute is transferred back into the mobile domain causing the concentration rebound observed in the breakthrough curve.

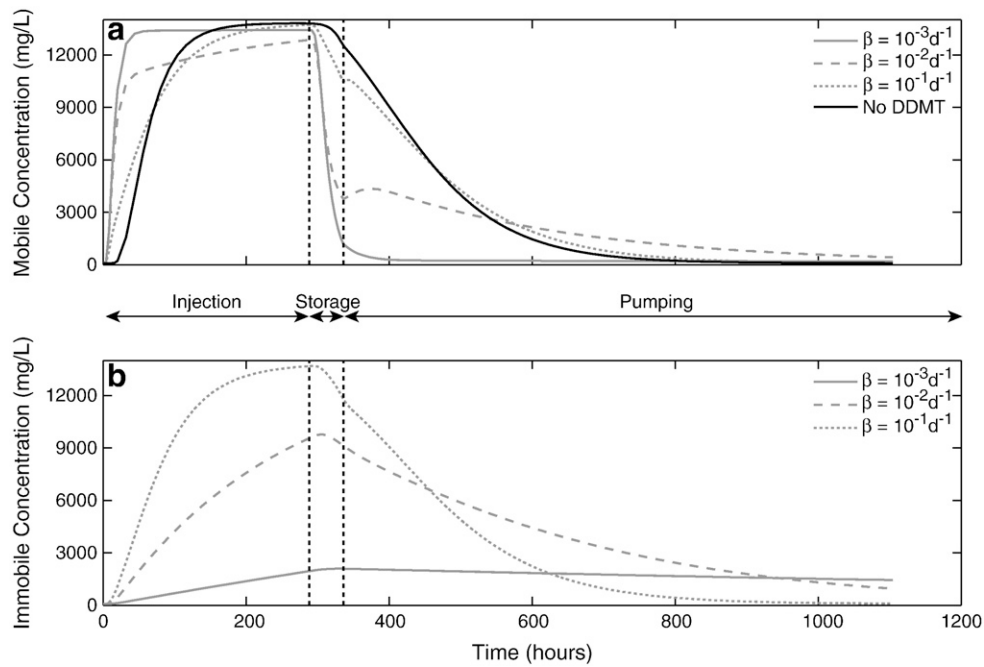


Fig. 3. (a) Mobile and (b) immobile concentrations through time at one point in space from a model with homogeneous hydraulic conductivity. Lower concentration peaks in the mobile zone exist for models with dual-domain mass transfer. The decrease in mobile porosity from the model without dual-domain mass transfer (10% porosity) to the model with dual-domain mass transfer (2.5% porosity) causes a corresponding increase in transport velocity resulting in earlier solute arrival times in the dual-domain mass transfer model; for the same reason, tailing behavior is comparatively suppressed. At high (10^{-1} /day) or low (10^{-3} /day) mass transfer rates, the mobile and immobile domains approach equilibrium and behavior is similar to a single-domain model. Deviation in equilibrium behavior is notable at intermediate mass transfer rates.

In the presence of dual-domain mass transfer, fluid and bulk apparent EC show hysteresis (Fig. 2). Bulk apparent EC is lower during the injection and early parts of the storage phases than expected from the mobile fluid EC, assuming Eq. (7), due to the remaining freshwater in the immobile domain. Bulk apparent EC is greater than expected during the pumping and late storage phases as the saline tracer moves into the immobile domain. As the transfer rate is increased, the lag between fluid and bulk EC increases, creating a wider hysteresis curve. However, at sufficiently fast rates ($1e-1$ /day; length scale of 0.9 m) the lag is reduced because the two domains equilibrate quickly and again act as a single domain with a total porosity equal to the mobile plus immobile porosities.

3.3. Effects of averaging and measurement of support volume

Archie's Law does not account for the fact that geophysical measurements have a larger support volume than the fluid EC, and consequently can 'see' solute that is outside of a sampling well; there is consequently the possibility that hysteresis is caused solely by a difference in scale between the measurements. To assess the ability of measurement support volume to cause hysteresis in the absence of heterogeneity, we constructed a homogeneous model with a constant background solute concentration of 85 mg/L. Using this model, we calculated the geometric factor for the electrode configurations used above. We then introduced the tracer via the injection/extraction well as described above and using the same electrode configuration, invoked the injection current, and calculated the voltage change, and we observed a deviation between the calculated bulk apparent EC using Eq. (10) and the bulk apparent EC estimated from the model (Fig. 2). We then repeated the experiment for the same background concentration, but varied the injection concentration, thus creating a difference in EC between the background and the plume, which would change the support volume of the measurement as the current paths change. In doing so, we found that the shape of this deviation between

the true and calculated bulk apparent EC is consistent for all the injection concentrations. Importantly, no hysteresis between bulk apparent and true EC is seen in any of these numerical models, which means that for the models, presented here, the observed hysteresis is caused by transport processes, not the difference in support volume between fluid and bulk apparent EC.

4. Development of a discrete fracture model

To compare the above results to those from a system in which macroscopic permeability heterogeneity may lead to anomalous transport, we develop a numerical model with a discrete fracture. A planar feature 0.2 m wide was emplaced at a depth of 36 m across the model domain to represent a fractured zone. Except for increasing the hydraulic conductivity within the fracture to 0.01 m/s, all other parameters are the same as in the homogeneous model, including a total assumed porosity of 0.1. The rate of mass transfer (β) is the same in both the fracture and matrix. An unstructured triangular mesh was sequentially generated outward, resulting in element properties similar to that of the homogeneous model; however, due to the small elements within the fracture, this model contained 17,669 triangular elements (Fig. 4). Model parameters are summarized in Table 2.

4.1. Modeling classical advective–dispersive behavior

The fracture simulation using the advective–dispersive equation produces skewed solute arrival times, elongated tailing and a second peak (Fig. 5). Notably, the discrete fracture results in hysteresis without the presence of diffusive mass transfer (Fig. 6). The disequilibrium is a result of the difference in concentration in the fracture versus that in the surrounding matrix. Initially, the solute moves rapidly through the fracture while the solute in the surrounding matrix rock lags behind; the fluid EC is consequently high while the bulk EC is comparatively low because the rest of the volume

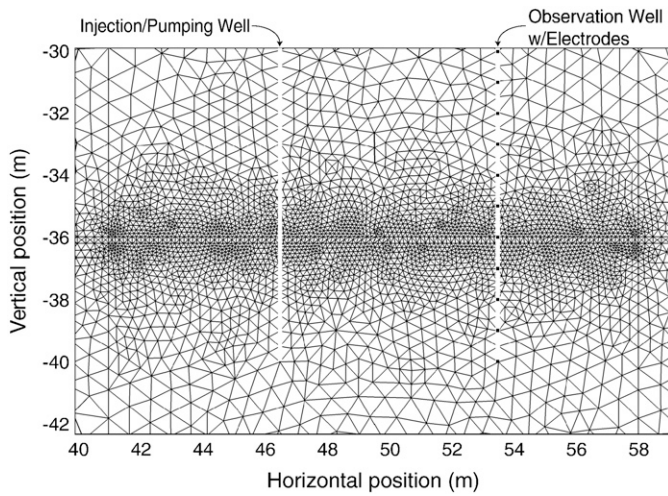


Fig. 4. Mesh used in the fracture at 36-m depth and in the vicinity of the pumping/injection and observation wells. Well locations are white and electrodes are represented with black rectangles.

supported by the bulk measurement still has a low solute concentration. In the storage phase, solute concentration in the fracture swiftly declines as the solute source is shut off, but the solute in the matrix lags, resulting in a higher concentration outside the fracture. Hence, bulk apparent EC is greater than predicted from the fluid EC because solute concentrations in the matrix are now high compared to the fracture. The rapid removal of the solute during the pumping phase leads to decreases in fluid and bulk apparent EC in the fracture and matrix. We observe a sharp increase in fluid EC in the fracture at the transition between storage and pumping phases, which suggests when pumping begins, the solute is rapidly advected through the fracture zone resulting in an increase in observed fluid EC. The bulk apparent EC continues to decrease during pumping, but otherwise, the bulk apparent EC data mimic the breakthrough data. Macroscopic heterogeneity of sufficient magnitude and spatial extent produces hysteresis.

4.2. Modeling dual-domain mass transfer

Taking the numerical model above with a discrete fracture, we add dual-domain mass transfer by assigning an immobile porosity of 0.075, a mobile porosity of 0.025, and a mass transfer rate of 10^{-2} /day

Table 2

Physical parameters used in the discrete fracture numerical models of flow, transport, and electrical conduction.

Storage term (S)	$3e-5 \text{ m}^{-1}$
Hydraulic conductivity, fracture (K)	0.01 m/s
Hydraulic conductivity (K)	$1.15e-4 \text{ m/s}$
Hydraulic gradient	0.02
Injection rate	0.07 L/s
Pumping rate	0.095 L/s
Total porosity (Φ_m)	0.1
Dispersivity, primary direction (mobile, α_1)	1 m
Dispersivity, secondary direction (mobile, α_2)	0.1 m
Tortuosity factor (τ_L)	1
Coefficient of molecular diffusion (D_L)	$1e-6 \text{ m}^2/\text{s}$
Initial solute concentration	85 mg/L
Injection concentration	16,000 mg/L
Current driven	1 A/m
Cementation factor	2
Mass transfer rate (β)	$1e-3/\text{day}-1e-2/\text{day}$
Mobile porosity (Φ_m)	0.025
Immobile porosity (Φ_{im})	0.075
Dispersivity, primary direction (immobile, α_1)	0 m
Dispersivity, secondary direction (immobile, α_2)	0 m

to both the fracture and matrix. The shape of the breakthrough curve for this scenario differs from the case of the discrete fracture without dual-domain mass transfer in two main ways (Fig. 5): (1) solute concentrations during the injection and storage phases in the mobile domain for this case are lower than in the case without dual-domain mass transfer, which is expected because the solute is being transferred into the immobile domain; and (2) this case creates a concentration history with a much more elongated tail than occurs considering advection–dispersion alone. We also observe hysteresis between fluid and bulk EC, but this curve differs from the case where no diffusive mass transfer occurs by having a larger lag between fluid and bulk apparent EC, a persistent lag throughout both storage and pumping periods, and a lower bulk electrical conductivity during injection (Fig. 6). The kink in the hysteresis curve at the transition between storage and pumping phases remains; it is an advective effect between the fracture and matrix.

We also tested two cases where the fracture and matrix had different mass transfer rates. In one model, the matrix had a transfer of $1e-3/\text{day}$ (approximating a length scale of mass transfer of ~ 9 m) while the fracture had a mass transfer rate of $1e-2/\text{day}$ (approximating a length scale of mass transfer of ~ 3 m), while in the second model the rate of mass transfer in the matrix was $1e-2/\text{day}$, and the rate of transfer in the fracture was $1e-1/\text{day}$ (approximating a length scale of mass transfer of 0.9 m). Increasing the mass transfer rate in the fracture by an order of magnitude beyond that used in the matrix resulted in breakthrough and EC behavior similar to the models with a single rate of mass transfer. EC and breakthrough behaviors were similar based upon the mass transfer rate in the matrix of the models, suggesting that the mass transfer rate of the matrix controls the observed hysteresis.

The disequilibrium produced by models with and without diffusive mass transfer are different when compared side-by-side. The disequilibrium caused by the fracture alone occurs over a shorter time-span and is smaller in magnitude, indicative of the small scale of mass transfer assumed. The lag caused by the advective effects of the fracture is imprinted upon the disequilibrium caused by dual-domain mass transfer, and manifests as a wider, smooth hysteresis that starts in the injection period and persists throughout the storage and pumping periods, indicative of both this small-scale mass transfer, and disequilibrium created by the presence of the 0.2 m-wide fracture.

5. Development of a heterogeneous hydraulic conductivity model

To explore the impact of dual-domain mass transfer on electrical signatures given a different type of heterogeneity, we develop a heterogeneous hydraulic conductivity model based on sequential Gaussian simulation. SGSIM (Deutsch and Journel, 1998) was used to create a random hydraulic conductivity field 27 m wide and 46 m tall with a grid spacing of 0.25 m which was centered on the pumping and observation wells (Fig. 7). The geometric mean of the hydraulic conductivity is $5.96e-4 \text{ m/s}$, the variance of the natural log of the hydraulic conductivity is 1.2, and the correlation length is 2.25 m. The hydraulic conductivity is set at $1.15e-4 \text{ m/s}$ throughout the rest of the model domain. The hydraulic conductivity field was then interpolated to the mesh, which contained 9890 elements. The model geometry and all other parameters are identical to those used in the homogeneous model. Modeling parameters are summarized in Table 3.

5.1. Modeling classical advective–dispersive behavior

When considering advective–dispersive behavior in this heterogeneous field, the tracer breakthrough appears non-Fickian (Fig. 8). Plume snapshots indicate preferential fluid pathways, which are expected given the variations in the hydraulic conductivity. The bulk apparent EC data also indicates preferential fluid pathways. While more subtle than the discrete fracture case without mass transfer present, the relation between the bulk apparent and fluid EC exhibits

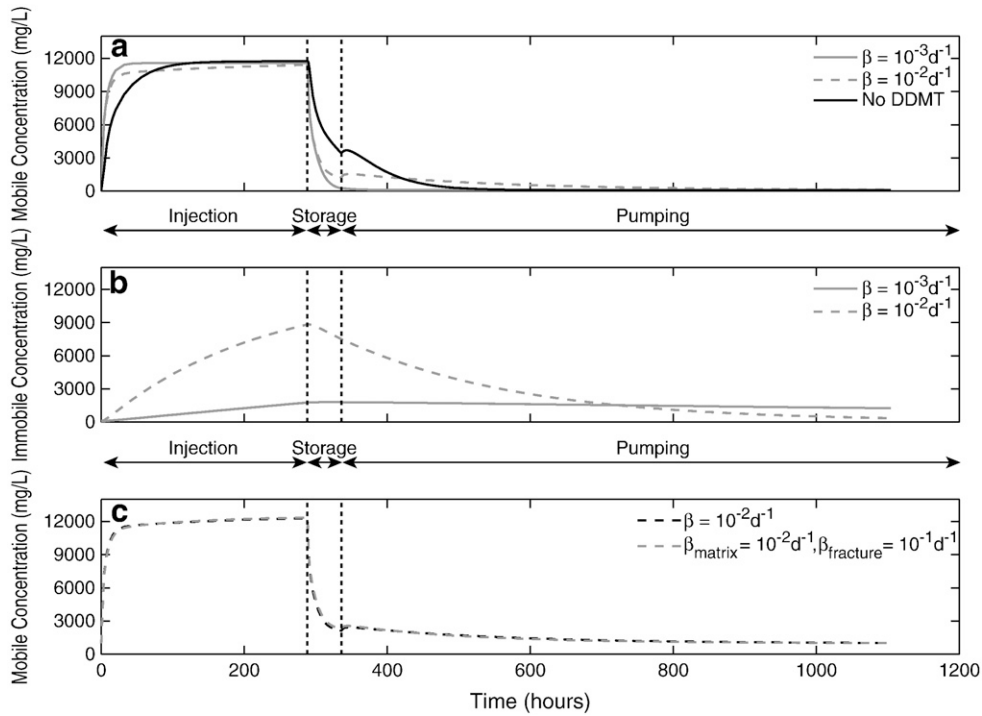


Fig. 5. (a) Mobile and (b) immobile concentrations from a point within the discrete fracture. Without dual-domain mass transfer, concentration rebound is observed at the beginning of the pumping period due to solute being pulled back through the fracture. Introducing dual-domain mass transfer (thus lowering the mobile porosity from 0.1 to 0.025, in these models) hastens solute arrival times. With dual-domain mass transfer, lower peak concentrations and longer tails are observed. (c) Mobile domain concentrations for models with a homogenous mass transfer rate versus those with differing mass transfer rates between the matrix and fracture are nearly identical.

hysteresis (Fig. 9). As seen in the fracture modeling, macroscopic heterogeneity produces hysteresis associated with the variability in hydraulic conductivity alone.

5.2. Modeling dual-domain mass transfer

Given the model above, we now add mass transfer by assuming an immobile porosity of 0.075, a mobile porosity of 0.025, and a range of

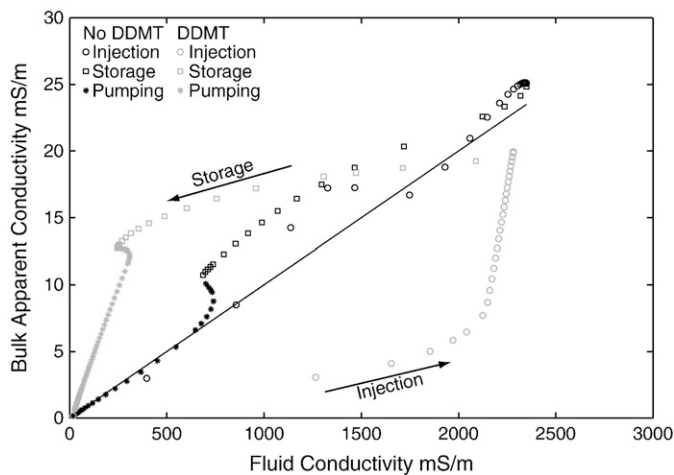


Fig. 6. Simulated bulk apparent and fluid EC for with a point within the discrete fracture. The black line is the true relation between bulk apparent and fluid EC used in the model. Discrete fracture zones result in hysteresis between bulk and fluid EC without explicitly invoking mass transfer processes (black symbols). Introducing dual-domain mass transfer (DDMT) increases the hysteresis (gray symbols). During the injection period, the hysteresis curve in the presence of dual-domain mass transfer is below the true relation between fluid and bulk apparent EC because the immobile domain (7.5% porosity) is relatively fresh compared to the mobile domain (2.5% porosity).

mass transfer rates. Breakthrough curves exhibit longer tails because solute has been transferred into the immobile domain (Fig. 8). As the mass transfer rate increases from 1e-2/day from 1e-3/day, the amount of solute transferred into the immobile domain increases. Plume snapshots still indicate preferential pathways from the permeability heterogeneity. Notably, areas of lower hydraulic conductivity have a higher bulk apparent EC for longer time periods because these areas allow the mobile and immobile zones more time to transfer solutes. Again, we observe hysteresis curves caused by dual-domain mass transfer with the effects of larger-scale heterogeneity imprinted upon them (Fig. 9). With mass transfer rates greater than 1e-3/day, we observe a rebound in concentration in the breakthrough and EC

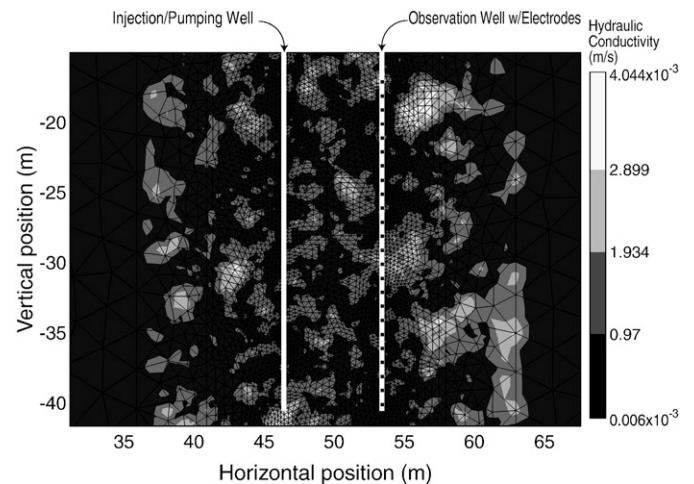


Fig. 7. Mesh used in the heterogeneous K-field simulations in the vicinity of the pumping/injection and observation wells. Well locations are white and electrodes are represented with black rectangles.

Table 3

Physical parameters used in the heterogeneous numerical models of flow, transport, and electrical conduction.

Storage term (S)	$3e-5 \text{ m}^{-1}$
Average hydraulic conductivity (K)	$5.96e-4 \text{ m/s}$
Hydraulic gradient	0.02
Injection rate	0.07 L/s
Pumping rate	0.095 L/s
Total porosity (Φ_m)	0.1
Dispersivity, primary direction (mobile, α_1)	1 m
Dispersivity, secondary direction (mobile, α_2)	0.1 m
Tortuosity factor (τ_L)	1
Coefficient of molecular diffusion (D_L)	$1e-6 \text{ m}^2/\text{s}$
Initial solute concentration	85 mg/L
Injection concentration	16,000 mg/L
Current driven	1 A/m
Cementation factor	2
Mass transfer rate (β)	$1e-3/\text{day} - 1e-1/\text{day}$
Mobile porosity (Φ_m)	0.025
Immobile porosity (Φ_{im})	0.075
Dispersivity, primary direction (immobile, α_1)	0 m
Dispersivity, secondary direction (immobile, α_2)	0 m

curves at the beginning of the pumping period caused by solute being transferred back into the mobile domain. When the mass transfer rate is increased to $1e-1/\text{day}$, the lag between mobile and immobile domains decreases and the system begins to appear more similar to a single-domain case.

6. Discussion and model relevance to field studies

Our modeling demonstrates that macroscopic heterogeneity as well as solute mass transfer creates hysteresis between bulk apparent and fluid EC data, and that the magnitude of hysteresis is a function of the scale of solute mass transfer. While separating advective and diffusive behavior may be difficult in field data, the disconnect

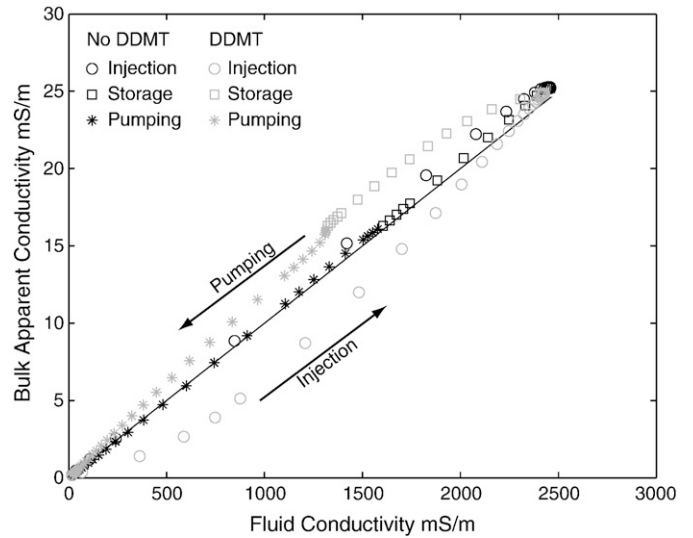


Fig. 9. Simulated bulk apparent and fluid EC for a model with heterogeneous hydraulic conductivity. The black line is the true relation between bulk apparent and fluid EC used in the model. Heterogeneity in hydraulic conductivity ($\text{var}(\ln(K)) = 1.2$), without dual-domain mass transfer (DDMT), results in a slight hysteresis between fluid and bulk apparent EC without invoking mass transfer processes explicitly (black symbols). The addition of dual-domain mass transfer at a rate of $10^{-1}/\text{day}$ (gray symbols) increases the hysteresis, as would be expected. The hysteresis observed here is smaller than the previous two cases because the high rate of mass transfer keeps the mobile and immobile domains closer to equilibrium.

between fluid and bulk EC data could be used to estimate properties like mass transfer rates or the volume of immobile pore space. However, to analyze these values in a meaningful way would require an understanding of the site geology and expected heterogeneity. For example, fracture sets can occur as groups of tens to thousands of

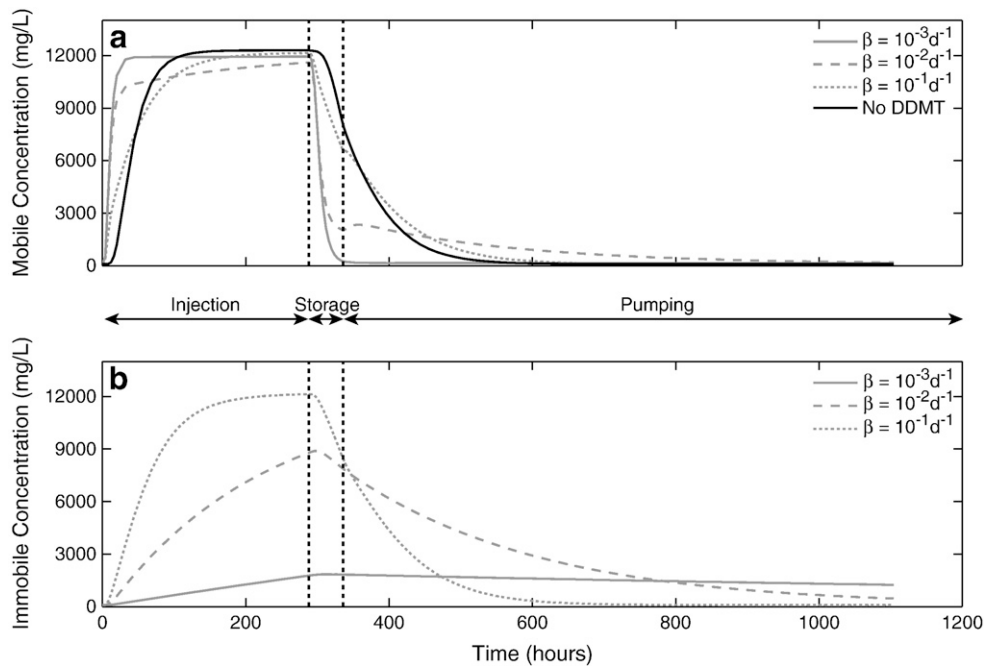


Fig. 8. (a) Mobile and (b) immobile concentration at one point in space from the model with heterogeneous hydraulic conductivity. Although solute plume snapshots (not shown here) demonstrate preferential pathways, solute behavior in the mobile domain is similar to the homogeneous case. Introducing dual-domain mass transfer (thus lowering the mobile porosity from 0.1 to 0.025, in these models) hastens solute arrival times and produces tailing behavior similar to the homogeneous case. At low ($10^{-3}/\text{day}$) or high ($10^{-1}/\text{day}$) mass transfer rates, the mobile and immobile domains approach equilibrium and concentration behavior is similar to the single-domain case. Intermediate transfer rates result in deviation from equilibrium behavior such as the rebound observed at the beginning of the pumping period. With dual-domain mass transfer, mobile domain concentration peaks are lower and longer tails are observed.

individual fractures in the field; it is therefore likely in highly fractured media that the magnitude of hysteresis is smaller than in cases where only a small proportion of large-scale fractures may be relevant for conducting fluids (Long et al., 1991; Renshaw, 1995; Hsieh and Shapiro, 1996). Based on our model results, we conclude that the shape of the hysteresis curve in field settings tells us about variations in the length scales of heterogeneity controlling transport. In general, the results from both the dual-domain mass transfer and heterogeneity models indicate that as the length scale of the heterogeneity decreases, so does the magnitude of the hysteresis. The heterogeneous hydraulic conductivity model with a correlation length of 2.25 m produces hysteresis quite different from models with an intermediate mass transfer rate of $1e-2/\text{day}$ (infers a diffusive mixing scale of ~ 3 m), suggesting that the length scale inferred from mass transfer is not simply a function of correlation length, but likely also a function of geometry of the heterogeneity.

We should note that these models cannot be fully representative of field processes, in part because of the dimensionality of the modeling, but also because field data are complicated by the effects of fine-scale heterogeneity in hydraulic conductivity or mass transfer parameters, which are not considered here. For example, we chose to use a single rate of mass transfer in our models, although many other studies have utilized multiple rates of mass transfer. Quantification of mass transfer processes at multiple scales in field settings may be possible, but would be dependent on collecting multiscale geophysical data. Another simplification in our model was to use a conservative tracer that did not impact surface conductance; the consideration of this process would change the hysteresis observed between bulk and fluid EC. We also note that the time-scale of observation affects the role that heterogeneity played in producing hysteresis between bulk and fluid EC. In the discrete fracture model, solute traveling strictly through the matrix broke through at the observation well and the resulting difference between concentration in the matrix and fracture caused the observed hysteresis. If we reduced the model simulation time, solute moving strictly through the matrix would not have enough time to reach the observation well and the hysteresis caused by large-scale heterogeneity would be absent. Additionally, the diffusion coefficient used here is larger than the open-water diffusion of many ions; adjustment of this parameter in the models would change the estimated length scale of diffusion. Despite these simplifications, we can reproduce a disconnect between the fluid and bulk apparent EC similar to that observed by Singha et al. (2007) in the field given either macroscopic heterogeneity or small-scale mass transfer, and demonstrate that the disconnect is driven by the length scales of heterogeneity, which may be information that is exploitable in field settings.

7. Conclusions

Previous studies have highlighted the complexity associated with interpreting solute transport processes from limited measurements of point-scale fluid chemistry data, and that geophysical data may be useful in estimating mass transfer rates and immobile porosities in situ. Our modeling results indicate that subscale dual-domain mass transfer and macroscopic heterogeneity both produce a measurable hysteresis between fluid and bulk apparent EC. The hysteresis is controlled by the geometry of low permeability material, the mass transfer rate, and the aquifer porosity, which means that the curve shape is indicative of the length scale over which mass transfer is occurring. As previously noted, there are factors that may contribute to hysteresis that are outside the scope of the study presented here. For these examples, the curve shape is indicative of the length scale over which mass transfer is occurring. In field settings, the shape of the curve will also be dependent on many other factors such as pumping rates, relative magnitudes of hydraulic properties, and boundary conditions.

While quantifying advective versus diffusively controlled transport can be ambiguous from these data, we note that the disequilibrium between fluid EC and bulk EC data is indicative of mass transfer processes at some scale, and provides a manner for estimating mass transfer rates between domains and the volume of immobile pore space as shown in Day-Lewis and Singha (2008). Collecting multiscale geophysical data may be key to determining how the rates of mass transfer change with scale. In cases where good information on site geology exists such that the macroscopic heterogeneity is well characterized, electrical measurements may be used to help discern advective versus diffusive controls on transport.

Acknowledgements

This material is based upon work supported by the National Science Foundation (NSF) under Grant No. EAR-0747629 and the American Chemical Society PRF Grant 45206-G8. Any opinions, findings and conclusions or recommendations expressed in this material are those of the author and do not necessarily reflect the views of the NSF. DDW would like to thank Fred Day-Lewis, Derek Elsworth, Maggie Popek, Christine Regalla, and Brad Kuntz for insightful discussions.

References

- Adams, E.E., Gelhar, L.W., 1992. Field study of dispersion in a heterogeneous aquifer 2. Spatial moments analysis. *Water Resour. Res.* 28 (12), 3293–3307. doi:10.1029/92WR01757.
- Archie, G.E., 1942. The electrical resistivity log as an aid in determining some reservoir characteristics: transactions of the American Institute of Mining. *Metall. Pet. Eng.* 146, 54–62.
- Barlebo, H.C., Hill, M.C., Rosbjerg, D., 2004. Investigating the Macrodispersion Experiment (MADE) site in Columbus, Mississippi, using a three-dimensional inverse flow and transport model. *Water Resour. Res.* 40 (4), 1–18. doi:10.1029/2002WR001935.
- Bear, J., 1972. *Dynamics of Fluids in Porous Media*. Elsevier Publishing Company.
- Becker, M.W., Shapiro, A.M., 2000. Tracer transport in fractured crystalline rock: evidence of nondiffusive breakthrough tailing. *Water Resour. Res.* 36 (7), 1677–1686. doi:10.1029/2000WR900080.
- Becker, M.W., Shapiro, A.M., 2003. Interpreting tracer breakthrough tailing from different forced-gradient tracer experiment configurations in fractured bedrock. *Water Resour. Res.* 39 (1), 1–13. doi:10.1029/2001WR001190.
- Benson, D.A., Wheatcraft, S.W., Meerschaert, M.M., 2000. The fractional-order governing equation of Levy motion. *Water Resour. Res.* 36 (6), 1413–1423. doi:10.1029/2000WR900032.
- Berkowitz, B., Scher, H., 1995. On characterization of anomalous dispersion in porous and fractured media. *Water Resour. Res.* 31 (6), 1461–1466. doi:10.1029/95WR00483.
- Berkowitz, B., Scher, H., 2001. The role of probabilistic approaches to transport theory in heterogeneous media. *Transp. Porous Media* 42 (1), 241–263. doi:10.1023/A:1006785018970.
- COMSOL, 2006. *COMSOL Multiphysics User's Guide*. COMSOL AB, Burlington, MA, USA. 708 pp.
- Cortis, A., Berkowitz, B., 2004. Anomalous transport in "classical" soil and sand columns. *Soil Sci. Soc. Am. J.* 68 (5), 1539–1548.
- Day-Lewis, F.D., Lane, J.W., Gorelick, S.M., 2006. Combined interpretation of radar, hydraulic, and tracer data from a fractured-rock aquifer near Mirror Lake, New Hampshire, USA. *Hydrogeol. J.* 14 (1), 1–14. doi:10.1007/s10040-004-0372-y.
- Day-Lewis, F.D., Singha, K., 2008. Geoelectrical inference of mass transfer parameters using temporal moments. *Water Resour. Res.* 44 (5), 1–6. doi:10.1029/2007WR006750.
- Dentz, M., Tartakovsky, D.M., 2006. Delay mechanisms of non-Fickian transport in heterogeneous media. *Geophys. Res. Lett.* 33 (16), 1–5. doi:10.1029/2006GL027054.
- Deutsch, C.V., Journel, A.G., 1998. *GSLIB Geostatistical Software Library and User's Guide*. Oxford University Press, New York. 369 pp.
- Feehley, C.E., Zheng, C., Molz, F.J., 2000. A dual-domain mass transfer approach for modeling solute transport in heterogeneous aquifers: application to the Macrodispersion Experiment (MADE) Site. *Water Resour. Res.* 36 (9), 2501–2515. doi:10.1029/2000WR900148.
- Haggerty, R., Gorelick, S.M., 1994. Design of multiple contaminant remediation: sensitivity to rate-limited mass transfer. *Water Resour. Res.* 30 (2), 435–446. doi:10.1029/93WR02984.
- Haggerty, R., Gorelick, S.M., 1995. Multiple-rate mass transfer for modeling diffusion and surface reactions in media with pore-scale heterogeneity. *Water Resour. Res.* 31 (10), 2383–2400. doi:10.1029/95WR10583.
- Harvey, C., Gorelick, S.M., 2000. Rate-limited mass transfer or macrodispersion: which dominates plume evolution at the Macrodispersion Experiment (MADE) Site? *Water Resour. Res.* 36 (3), 637–650.
- Hill, M.C., Barlebo, H.C., Rosbjerg, D., 2006. Reply to comment by F. Molz et al. on Investigating the Macrodispersion Experiment (MADE) site in Columbus, Mississippi, using a three-dimensional inverse flow and transport model. *Water Resour. Res.* 42 (6), 1–4. doi:10.1029/2005WR004624.

- Hsieh, P.A., Shapiro, A.M., 1996. Hydraulic characteristics of fractured bedrock underlying the FSE well field at the Mirror Lake Site, Grafton County, New Hampshire. U.S. Geological Survey Toxic Substances Hydrology Program-Proceedings of the technical meeting, Colorado Springs, Colorado, September 20–24, 1993, U.S. Geol. Surv. Water-Resour. Invest. Rep. 94–4015, 127–130.
- Keller, G.V., Frischknecht, F.C., 1966. *Electrical Methods in Geophysical Prospecting*. Pergamon Press, Oxford, U.K. 523 pp.
- Levy, M., Berkowitz, B., 2003. Measurement and analysis of non-Fickian dispersion in heterogeneous porous media. *J. Contam. Hydrol.* 64 (3–4), 203–226. doi:10.1016/S0169-7722(02)00204-8.
- Long, J.C.S., Karasaki, K., Davey, A., Peterson, J., Landsfeld, M., Kemeny, J., et al., 1991. An inverse approach to the construction of fracture hydrology models conditioned by geophysical data: an example from the validation exercises at the Stripa Mine. *Int. J. Rock Mech. Min. Sci. Geomech. Abstr.* 28 (2–3), 121–142. doi:10.1016/0148-9062(91)92162-R.
- Molz, F.J., Zheng, C., Gorelick, S.M., Harvey, C.F., 2006. Comment on “Investigating the Macrodispersion Experiment (MADE) site in Columbus, Mississippi, using a three-dimensional inverse flow and transport model” by Heidi Christiansen Barlebo, Mary C. Hill, and Dan Rosbjerg. *Water Resour. Res.* 42 (6), 1–5. doi:10.1029/2005WR004265.
- Renshaw, C.E., 1995. On the relationship between mechanical and hydraulic aperture in rough-walled fractures. *J. Geophys. Res.* 100 (B12), 24629–24636.
- Sánchez-Vila, X., Carrera, J., 2004. On the striking similarity between the moments of breakthrough curves for a heterogeneous medium and a homogeneous medium with a matrix diffusion term. *J. Hydrol.* 294 (1–3), 164–175. doi:10.1016/j.jhydrol.2003.12.046.
- Singha, K., Day-Lewis, F.D., Lane Jr., J.W., 2007. Geoelectrical evidence of bicontinuum transport in groundwater. *Geophys. Res. Lett.* 34 (12), 1–5. doi:10.1029/2007GL030019.
- Singha, K., Gorelick, S.M., 2006. Hydrogeophysical tracking of three-dimensional tracer migration: the concept and application of apparent petrophysical relations. *Water Resour. Res.* 42 (6), 1–14. doi:10.1029/2005WR004568.
- Singha, K., Pidlisecky, A., Day-Lewis, F.D., Gooseff, M.N., 2008. Electrical characterization of non-Fickian transport in groundwater and hyporheic systems. *Water Resour. Res.* 44, 1–14. doi:10.1029/2008WR007048.
- Slater, L., Binley, A.M., Daily, W., Johnson, R., 2000. Cross-hole electrical imaging of a controlled saline tracer injection. *J. Appl. Geophys.* 44 (2–3), 85–102. doi:10.1016/S0926-9851(00)00002-1.